

TenDSuR: Tensor-Based 4D Sub-Nyquist Radar

Siqi Na ^{ID}, Kumar Vijay Mishra ^{ID}, Senior Member, IEEE, Yimin Liu ^{ID}, Member, IEEE,
Yonina C. Eldar ^{ID}, Fellow, IEEE, and Xiqin Wang

Abstract—We propose tensor-based four-dimensional sub-Nyquist radar that samples in spectral, spatial, Doppler, and temporal domains at sub-Nyquist rates while simultaneously recovering the target’s direction, Doppler velocity, and range without loss of native resolutions. We formulate the radar signal model wherein the received echo samples are represented by a partial third-order tensor. We then apply compressed sensing in the tensor domain and use our tensor-orthogonal matching pursuit (OMP) and tensor completion algorithms for signal recovery. Our numerical experiments demonstrate joint estimation of all three target parameters at the same native resolutions as a conventional radar but with reduced measurements. Furthermore, tensor completion methods show enhanced performance in off-grid target recovery with respect to tensor-OMP.

Index Terms—Canonical polyadic decomposition, MIMO, PARAFAC, radar, sub-Nyquist, tensor decomposition.

I. INTRODUCTION

IN RECENT years, radar systems that use fewer measurements in temporal, spectral, Doppler or spatial signal domains and yet achieve identical or even better performance than conventional systems, have captured significant interest [1]–[3]. The savings in metrics such as antenna aperture, bandwidth, sampling rate or dwell time lead to low cost and small size systems that are not very demanding on data throughput. Furthermore, reduction in system resources enables the radar to share them among different applications. For instance, technologies like multi-function integrated radio-frequency (RF) aperture systems [4]–[6], spectral coexistence [7], [8], cognitive radars [9], [10] and reconfigurable arrays [11] provide multiple services such as surveillance, tracking, and communication using a single system.

The literature indicates several different approaches towards realizing reduced-rate radars (see e.g. [2], [3], [12]–[14] and references therein) mostly based on compressed sensing (CS). In this work, we focus on those reduced-rate techniques which model the analog received radar signal utilizing the theory of

Manuscript received August 30, 2018; revised October 21, 2018; accepted November 20, 2018. Date of publication December 10, 2018; date of current version December 24, 2018. The work of K. V. Mishra was supported in part by Andrew and Erna Finci Viterbi Postdoctoral Fellowship and in part by Lady Davis Postdoctoral Fellowship. The work of Y. Liu was supported by the National Natural Science Foundation of China under Grant 61571260. The associate editor coordinating the review of this manuscript and approving it for publication was Dr. Pu Wang. (*Corresponding author: Yimin Liu*)

S. Na, Y. Liu, and X. Wang are with the Department of Electronic Engineering, Tsinghua University, Beijing 100084, China (e-mail: nasiqi123456@163.com; yiminliu@tsinghua.edu.cn; wangxq_ee@tsinghua.edu.cn).

K. V. Mishra and Y. C. Eldar are with the Andrew and Erna Viterbi Faculty of Electrical Engineering, Technion—Israel Institute of Technology, Haifa 3200003, Israel (e-mail: mishra@ee.technion.ac.il; yonina@ee.technion.ac.il).

Digital Object Identifier 10.1109/LSP.2018.2885617

finite-rate-of-innovation (FRI) [15]. These systems - referred to as sub-Nyquist radars - perform signal detection and parameter estimation from much fewer measurements than that required by Nyquist sampling and employ the Xampling framework [15] to obtain low-rate samples of the signal.

In the temporal domain, [16] proposed a sub-Nyquist radar to recover target delays relying on the FRI model. Similar techniques were later studied for delay channel estimation problems in ultra-wideband [17] and millimeter wave [18] communication systems. The *Doppler focusing* technique was added to the temporal sub-Nyquist radar in [19] to recover both delays and Dopplers. However, this system reduced samples only in time but not in the Doppler domain. The sub-Nyquist reduced time-on-target radar in [20] demonstrated dilution of samples in both the time and Doppler domains. For spatial compression, thinned arrays were examined for a multiple-input-multiple-output (MIMO) array radar in [21] and later for phased arrays in [5]. In [22], targets’ ranges, velocities, and directions were recovered in a new radar structure called Sub-Nyquist MIMO Radar (SUMMeR) by thinning a colocated MIMO array and collecting low-rate samples at each receiver element. The SUMMeR system was also implemented in a hardware prototype [9], [23].

In this work, motivated by recent advancements in exploring high-order data structure [24] in multidimensional harmonic retrieval [25], dictionary learning [26], channel sounding [27], and bistatic MIMO radar processing [28], we propose a Tensor-based four-dimensional (4D) Sub-Nyquist Radar (TenDSuR). TenDSuR compresses samples in spectral-spatial-Doppler-temporal (S-S-D-T) domains and processes the received echoes to jointly recover range, direction of arrival (DoA), and Doppler by applying tensor-based signal processing. There are a few CS-based approaches [12]–[14] which jointly estimate range, DoA, and Doppler but they do not reduce samples in all four S-S-D-T domains simultaneously. Furthermore, the complexity in these approaches is much larger than TenDSuR. The spatial compression in TenDSuR is achieved by deploying a thinned MIMO antenna as in [5], [22]. For spectral compression of transmit waveforms, we follow the ideas of [29], [30] and employ frequency-diversity waveforms which occupy only a fraction of the full bandwidth required to achieve the range resolution as in SUMMeR [22]. Temporal compression is accomplished at the sub-Nyquist receiver which recovers the target parameters via Xampling.

For Doppler compression, TenDSuR transmitters send agile waveforms with reduced number of pulses as in [20]. Thus, unlike SUMMeR, the TenDSuR system does not transmit pulses at a uniform pulse repetition interval (PRI). This leads to significant reduction in the total duration which each of the antenna elements are dedicated to a specific RF service. In addition, SUMMeR employs Doppler focusing, which is carried out over set of frequencies that are fixed *a priori*. The resultant Doppler

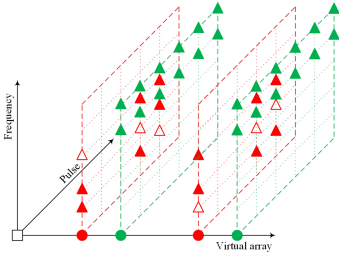


Fig. 1. Illustration of sub-Nyquist sampling. Different colors refer to different transmit antenna elements. The solid circles denote sampling instants along the virtual aperture. The triangles in one Frequency-Pulse plane indicate the measurements correspond to the same transmit and receive elements.

resolution is limited by the focusing, i.e., inversely proportional to the number of pulses P as is also the case with conventional radar. In contrast, the TenDSuR processing algorithm is based on tensor completion (TC) [31] leading to higher resolution recovery of the targets with off-grid range, Doppler, and DoA. The flexible signal model of TenDSuR is suitable for arbitrary waveforms. Our results show that in order to achieve the same detection performance in Doppler and DoA, TenDSuR requires fewer pulses per transmitter than SUMMeR [22]. When all pulses and frequency points are used, the TenDSuR signal model is equivalent to SUMMeR. However, for off-grid targets, TC-based recovery outperforms SUMMeR even when pulses are not diluted.

Throughout this letter, we use bold lowercase, bold uppercase and calligraphic letters for the vectors, matrices and tensors respectively. The s th column of matrix \mathbf{Y} is $[\mathbf{Y}]_s$; the submatrix of \mathbf{Y} that has columns specified by the index Π is $[\mathbf{Y}]_{\Pi}$; and the (i, j, k) th entry of a tensor \mathcal{Y} is $[\mathcal{Y}]_{i,j,k}$. The notations \otimes , \circ , and \diamond are the Kronecker, outer vector, and Khatri-Rao products, respectively; $|\cdot|$ is the element-wise magnitude or absolute value; $\llbracket \cdot \rrbracket$ is the multi-linear product; $(\cdot)^*$, $(\cdot)^T$, $(\cdot)^H$, and $\|\cdot\|_*$ denote conjugate, transpose, Hermitian and nuclear norm of a matrix, respectively. The notation $\mathcal{P}_{\Gamma}\{\cdot\}$ selects only those entries of its argument that are listed within the index set Γ ; $\mathcal{H}\{\cdot\}$ transforms a vector to its corresponding Hankel matrix and $\text{vec}(\cdot)$ vectorizes a tensor by stacking its matrices column-wise.

II. SYSTEM MODEL

Consider a traditional collocated MIMO radar with full Nyquist sampling. The operating wavelength of the radar is λ and the total number of transmit and receive elements are T and R , respectively. The MIMO antenna adopts a virtual uniform linear array (ULA) structure, with receive antennas spaced $\lambda/2$ and transmit antennas spaced by $R\lambda/2$. The coherent processing of a total of TR channels in the receiver creates a virtual equivalent of a phased array antenna that has TR elements each spaced $\lambda/2$ distance apart.

As shown in Fig. 1, spatial compression is realized by a thinned array, which has $M < T$ transmit and $Q < R$ receive antennas, as in [22]. The m th transmitting antenna is located at $\xi_m \lambda/2$, and the q th receive antenna is located at $\zeta_q \lambda/2$, where ξ_m and ζ_q are integers. The pulse train sent by the m th transmitting antenna over a coherent processing interval (CPI) spanning a duration of P pulses is

$$s_m(t) = \sum_{p=0}^{P-1} \delta_m[p] \cdot h_m^p(t - p\tau) e^{j2\pi f_c t}, \quad 0 \leq t \leq P\tau, \quad (1)$$

where τ denotes the PRI, $P\tau$ is the CPI, $f_c = c/\lambda$ is the common carrier frequency, c is the speed of light, $\delta_m[p] = 1$ or 0 indicates whether in the p th PRI, the m th transmitter emits a pulse or not. The waveform sent by the m th antenna in the p th PRI, $h_m^p(t)$, can vary between pulses for the spectral compression. For the p th PRI, $\{h_m^p(t)\}_{m=0}^{M-1}$ is a set of narrowband, orthogonal pulses each with continuous-time Fourier transform (CTFT) $H_m^p(\omega) = \int_{-\infty}^{\infty} h_m^p(t) e^{-j\omega t} dt$.

In TenDSuR, only $P_m < P$ pulses are emitted by each transmitter in a CPI and $\delta_m[p]$ can admit different values for the same p and different m . In SUMMeR, $\delta_m[p]$ is always unity for all m and p . We define the total duration for which the antenna elements are dedicated to a specific RF service as the aperture occupancy, $\text{AO} = \sum_{m=0}^{M-1} P_m$.

Suppose there exist L non-fluctuating point targets (Swerling-0 model), where the l th target is characterized by its complex reflectivity α_l , range r_l , radial velocity v_l , DoA $\vartheta_l = \sin \theta_l$, and θ_l is the azimuth. As derived in [22], the received echo of the p th pulse at the q th receiving antenna can be represented by its Fourier series, as

$$x_q^p(t) = \sum_n c_q^p[n] e^{-j2\pi n t / \tau}, \quad (2)$$

for $-NT/2 \leq n \leq NT/2 - 1$, with $N = B_h \tau$. Here,

$$c_q^p[n] = \frac{1}{\tau} \sum_{m=0}^{M-1} \sum_{l=1}^L \delta_m[p] \cdot \alpha_l e^{j2\pi \beta_{m,q} \vartheta_l} e^{-j\frac{2\pi}{\tau} n \tau_l} e^{-j2\pi f_l^D p \tau} H_m^p \left(\frac{2\pi}{\tau} n \right), \quad (3)$$

where the time delay $\tau_l = 2r_l/c$ is proportional to the l th target's range r_l , $f_l^D = 2\frac{v_l}{c} f_c$ is the Doppler frequency, and $\beta_{m,q} = (\zeta_q + \xi_m)(f_m \frac{\lambda}{c} + 1)$ is governed by the array structure.

We now apply Xampling in time, pulses and space to obtain low-rate samples of the received signal. The sampling technique is the same as in temporal sub-Nyquist radar [19], except that now the samples are obtained in the range, Doppler and azimuth domains. The received signal $x_q^p(t)$ is downconverted to baseband, separated into M channels, aligned and normalized. The Fourier coefficients of the received signal corresponding to the channel that processes the p th pulse of m th transmitter echo at the q th receiver are

$$\begin{aligned} y_{m,q}^p[k] &= \tau \left(H_m^p(2\pi k/\tau + f_m) \right)^* c_q^p[k + f_m \tau] / |H_0^0(2\pi k/\tau)|^2 \\ &= \sum_{l=1}^L \delta_m[p] \cdot \alpha_l e^{j2\pi \beta_{m,q} \vartheta_l} e^{-j\frac{2\pi}{\tau} k \tau_l} e^{-j2\pi f_m \tau_l} e^{-j2\pi f_l^D p \tau}. \end{aligned} \quad (4)$$

Here $-\frac{N}{2} \leq k \leq -\frac{N}{2} - 1$, f_m is the (baseband) carrier frequency of the m th transmitter, $c_q^p[k + f_m \tau]$ in (4) is exactly $c_q^p[n]$ in (3), and N is the number of Fourier coefficients per channel. Xampling obtains a set \mathcal{K} of arbitrarily chosen Fourier coefficients from low rate samples of the received channel signal such that $|\mathcal{K}| = K < N$.

Let \mathbf{Z}^m be the $KQ \times P_m$ matrix with q th column given by the vertical concatenation of $y_{m,q}^p[k]$, $k \in \mathcal{K}$, $0 \leq q \leq Q-1$ and $p \in \Pi_m$, where Π_m is the set of pulses chosen arbitrarily for transmission by the m th transmit antenna out of a total of P pulses such that $|\Pi_m| = P_m$. We can write \mathbf{Z}^m as

$$\mathbf{Z}^m = (\mathbf{B}^m \otimes \mathbf{A}^m) \mathbf{X}_D (\mathbf{F}^m)^T, \quad (5)$$

Algorithm 1: Construction of Index Sets Γ , Ω , Λ , and Π .

Input: $H_m^p(2\pi k/\tau)$
Output: Γ , Ω , Λ , Π

- 1: $\Gamma = \emptyset$, $\Omega = \emptyset$, $\Lambda = \emptyset$, $\Pi = \emptyset$;
- 2: **for** $m = 0$ to $M - 1$, $q = 0$ to $Q - 1$, $p = 0$ to $P - 1$, $k \in \mathcal{K}$ **do**
- 3: **if** $\delta_m[p] \cdot |H_m^p(2\pi k/\tau)| \neq 0$ **then**
- 4: $\Gamma = \Gamma \cup \{k + f_m \tau, \xi_m + \zeta_q, p\}$, $\Omega = \Omega \cup \{k + f_m \tau\}$, $\Lambda = \Lambda \cup \{\xi_m + \zeta_q\}$, $\Pi = \Pi \cup \{p\}$;

where \mathbf{A}^m denotes the $K \times TN$ matrix whose (k, n) th element is $e^{-j\frac{2\pi}{TR} \mathcal{K}_k n} e^{-j2\pi \frac{f_m}{B_h} \frac{n}{T}}$ with \mathcal{K}_k the k th element in \mathcal{K} , \mathbf{B}^m is the $Q \times TR$ matrix with (q, p) th element $e^{-j2\pi \beta_{m,q}(-1 + \frac{2}{TR}p)}$ and \mathbf{F}^m denotes the $P_m \times P$ partial Fourier matrix. The matrix \mathbf{X}_D is a $T^2 NR \times P$ sparse matrix that contains the values α_l at the L indices. In TenDSuR, the row size of partial Fourier matrix \mathbf{F}^m can be different across all m . However, in SUMMeR, \mathbf{F}^m is always a full Fourier matrix for all transmitters.

Vectorizing both sides of (5) gives $\text{vec}(\mathbf{Z}^m) = \text{vec}((\mathbf{B}^m \otimes \mathbf{A}^m) \mathbf{X}_D (\mathbf{F}^m)^T) = (\mathbf{F}^m \otimes \mathbf{B}^m \otimes \mathbf{A}^m) \text{vec}(\mathbf{X}_D)$. Consider a $K \times Q \times P_m$ tensor \mathcal{Z}^m such that $\text{vec}(\mathbf{Z}^m) = \text{vec}(\mathcal{Z}^m)$. Then, $\mathcal{Z}^m = [\![\mathcal{X}; \mathbf{A}, \mathbf{B}, \mathbf{F}]\!]$, where $\mathcal{X} \in \mathbb{C}^{TN \times TR \times P}$ such that $\text{vec}(\mathbf{X}_D) = \text{vec}(\mathcal{X})$.

The matrices \mathbf{A}^m , \mathbf{B}^m and \mathbf{F}^m are obtained by selecting K , Q and P_m rows, respectively, of their full counterparts: $TN \times TN$ matrix \mathbf{A} , $TR \times TR$ matrix \mathbf{B} and $P \times P$ matrix \mathbf{F} . Hence, the partial tensor \mathcal{Z}^m is obtained by selecting a total of $KQ \sum_{m=0}^{M-1} P_m$ entries from the corresponding full tensor $\mathcal{Z} = [\![\mathcal{X}; \mathbf{A}, \mathbf{B}, \mathbf{F}]\!]$ of size $TN \times TR \times P$.

For on-grid targets, the Fourier coefficients of the received signal are obtained from \mathcal{Z} as

$$\bar{\mathcal{Z}} = \mathcal{P}_{\Gamma}\{\mathcal{Z}\} = \mathcal{P}_{\Gamma}\{[\![\mathcal{X}; \mathbf{A}, \mathbf{B}, \mathbf{F}]\!]\}, \quad (6)$$

where $\bar{\mathcal{Z}}$ represents the entries of \mathcal{Z} specified by the set Γ (constructed as per Algorithm 1). Sets Ω , Λ and Π index the rows of \mathbf{A}^m , \mathbf{B}^m and \mathbf{F}^m selected from \mathbf{A} , \mathbf{B} and \mathbf{F} , respectively.

For continuous-valued parameters, the entries of $\bar{\mathcal{Z}}$ are

$$[\bar{\mathcal{Z}}]_{k+f_m \tau, \xi_m + \zeta_q, p} = \sum_{l=1}^L \alpha_l \cdot e^{j2\pi \beta_{m,q} \vartheta_l} e^{-j\frac{2\pi}{\tau} k \tau_l} e^{-j2\pi f_m \tau_l} e^{-j2\pi f_l^D p \tau}. \quad (7)$$

III. TARGET RECOVERY

We first derive the number of samples needed for perfect recovery of $\{\alpha_l, \vartheta_l, \tau_l, f_l^D\}_{l=1}^L$ or \mathcal{X} . In the results below, the total number of transceiver frequencies, antennas, and pulses equals the number of $\bar{\mathcal{Z}}$'s non-zero matrix slices obtained by fixing the first, second, and third index, respectively.

Theorem 1: The minimal total numbers of antenna channels, transceiver frequencies, and pulses required for perfect recovery

of \mathcal{X} with L on-grid targets in a noiseless setting are each no less than $2L$.

Proof: For all $k \in \mathcal{K}$, $m = 0, \dots, M - 1$, $p = 0, \dots, P - 1$, if $|H_0^0(2\pi k/\tau)|^2 \neq 0$, then the signal model in (6) can be unfolded as the following $KQ \sum_{m=0}^{M-1} P_m$ equations

$$[\bar{\mathcal{Z}}]_{k, \xi_m + \zeta_q, p} = (([\mathbf{F}^T]_p)^T \otimes ([\mathbf{B}^T]_{\xi_m + \zeta_q})^T \otimes ([\mathbf{A}^T]_k)^T) \text{vec}(\mathcal{X}). \quad (8)$$

According to the FRI theory and Lemma 1 in [22], the sparse tensor \mathcal{X} can be perfectly recovered provided

$$\min\{\text{spark}(([F^T]_{\Pi})^T), \text{spark}(([A^T]_{\Omega})^T), \text{spark}(([B^T]_{\Lambda})^T)\} > 2L.$$

For Ω , Λ , and Π , if the overall number of tranceived frequency points is larger than $2L$, then $\text{spark}(([A^T]_{\Omega})^T) > 2L$; if the overall number of antenna channels is larger than $2L$, then $\text{spark}(([B^T]_{\Lambda})^T) > 2L$; and if the overall number of pulses is larger than $2L$, then $\text{spark}(([F^T]_{\Pi})^T) > 2L$. ■

Theorem 2: The minimal total numbers of antenna channels, transceiver frequencies, and pulses required for perfect recovery of L off-grid targets in a noiseless setting are each no less than $2L$.

Proof: We first prove the necessary condition for the overall number of pulses. The cases for overall number of antenna channels and transceiver frequency points are similar. Consider the case where all targets have identical DoAs and ranges, as $\vartheta_l = \vartheta_0$, $\tau_l = \tau_0$. Then, from (4),

$$e^{j2\pi \tau_0(f_m \tau + k)/\tau} e^{j2\pi \vartheta_0(\xi_m + \zeta_q)} \tau \left(H_m^p(2\pi k/\tau + f_m) \right)^* \times c_q^p[k + f_m \tau] = |H_0^0(2\pi k/\tau)|^2 \sum_{l=1}^L \delta_m[p] \cdot \alpha_l e^{-j2\pi f_l^D p}. \quad (9)$$

Summing over $m = 0, \dots, M - 1$, $q = 0, \dots, Q - 1$, and $k \in \mathcal{K}$ on both sides yields

$$z'[p] = \sum_{l=1}^L \alpha_l e^{-j2\pi f_l^D p}, \quad (10)$$

where (11) shown at the bottom of this page. In (11), if there exists a pulse index p' such that for all $k \in \mathcal{K}$, $m = 0, \dots, M - 1$, the term $\delta_m[p'] \cdot |H_0^0(2\pi k/\tau)|^2$ in the denominator vanishes, then $z'[p']$ is undefined. Then, according to FRI theory, there are only $2L$ degrees of freedom in (10) thereby requiring no less than $2L$ overall pulses for a successful recovery of L targets. ■

The crucial difference between the above two theorems and their counterparts Theorems 3 and 4 in [22], is that in SUMMeR, all transmitters have to transmit no less than $2L$ pulses in one CPI. However, in TenDSuR, we need at least $2L$ pulses in a CPI but only one transmitter needs to be active. This significantly reduces the AO of an RF service.

For continuous target parameters, one could estimate the unknown parameters via TC [31] and parallel factor analysis

$$z'[p] = \frac{\sum_{m=0}^{M-1} \sum_{q=0}^{Q-1} \sum_{k \in \mathcal{K}} e^{j2\pi \tau_0(f_m \tau + k)/\tau} e^{j2\pi \vartheta_0(\xi_m + \zeta_q)} \left(H_m^p(2\pi k/\tau + f_m) \right)^* \cdot c_q^p[k + f_m \tau]}{Q \sum_{m=0}^{M-1} \sum_{k \in \mathcal{K}} \delta_m[p] \cdot |H_0^0(2\pi k/\tau)|^2} \quad (11)$$

(PARAFAC) [24] or higher order harmonic retrieval algorithms [25]. In this work, we utilize the Hankel Matrix nuclear norm Regularized low-CP-rank Tensor Completion (HMRTC) [32], which explores both low CP-rank and Vandermonde structure of \mathcal{Z} , to recover the targets' parameters:

$$\begin{aligned} \{\hat{\mathbf{a}}_l, \hat{\mathbf{b}}_l, \hat{\mathbf{f}}_l\}_{l=1}^L &= \arg \min_{\{\mathbf{a}_l, \mathbf{b}_l, \mathbf{f}_l\}_{l=1}^L} \sum_{l=1}^L \|\mathcal{H}\{\mathbf{a}_l\}\|_* + \|\mathcal{H}\{\mathbf{b}_l\}\|_* \\ &+ \|\mathcal{H}\{\mathbf{f}_l\}\|_* + \frac{\mu}{2} \left\| \mathcal{P}_\Gamma \left\{ \sum_{l=1}^L \mathbf{a}_l \circ \mathbf{b}_l \circ \mathbf{f}_l \right\} - \mathcal{P}_\Gamma \{\mathcal{Z}\} \right\|_2^2, \end{aligned} \quad (12)$$

where μ is a regularization parameter [32] and, as per (7),

$$\begin{aligned} \mathbf{a}_l &= \left[1, e^{-j2\pi\frac{\tau_l}{\tau}}, \dots, e^{-j2\pi(TN-1)\frac{\tau_l}{\tau}} \right]^T, \\ \mathbf{b}_l &= \left[1, e^{-j2\pi(f_m\frac{\lambda}{c}+1)\vartheta_l}, \dots, e^{-j2\pi(TR-1)(f_m\frac{\lambda}{c}+1)\vartheta_l} \right]^T, \\ \mathbf{f}_l &= \left[1, e^{-j2\pi f_l^D \tau}, \dots, e^{-j2\pi(P-1)f_l^D \tau} \right]^T. \end{aligned} \quad (13)$$

The target parameters are obtained after recovering $\{\hat{\mathbf{a}}_l, \hat{\mathbf{b}}_l, \hat{\mathbf{f}}_l\}_{l=1}^L$. For on-grid target parameters, the \mathcal{X} or \mathbf{x} is retrieved by solving the sparse recovery problem:

$$\min_{\mathcal{X}} \|\mathcal{X}\|_0 \text{ s.t. } \|\mathcal{P}_\Gamma\{\mathcal{X}; \mathbf{A}, \mathbf{B}, \mathbf{F}\} - \mathcal{P}_\Gamma\{\mathcal{Z}\}\|_2 \leq \varepsilon, \quad (14)$$

where ε is the error threshold determined by the noise power. Among several CS algorithms to solve this problem [33], we use orthogonal matching pursuit (OMP) [15], popular for its good trade-off between recovery accuracy and computational load. The details of the tensor version of OMP is omitted for length limitation. The computational complexity of HMRTC and tensor-OMP are $O(LI^3)$ (per iteration [32]) and $O(LT^2NRPI)$, respectively, where $I = \max\{TN, TR, P\}$.

IV. NUMERICAL EXPERIMENTS

In all our numerical experiments, a radar with full antenna aperture $TR = 20$, $\lambda = 0.03$ m, $P = 16$, and $\tau = 0.016$ ms was compressed by a thinned MIMO array with $M = 2$ transmit and $Q = 5$ receive elements with locations $\{0, \lambda/2\}$ and $\{\lambda, 5\lambda/2, 11\lambda/2, 13\lambda/2, 15\lambda/2\}$, respectively. The native range resolution corresponding to the full bandwidth is 150 m. Thus, $TN = 16$. We assume additive white Gaussian noise at each receiver with identical noise power. We consider the matched filter definition of the signal-to-noise-ratio, $\text{SNR} = \frac{(\sum_{m=0}^{M-1} \sum_{k \in \mathcal{K}} |H_0^0(2\pi k/\tau)|)^2}{\sigma^2 \cdot K Q \sum_{m=0}^{M-1} P_m}$, where σ^2 is the noise power in the bandwidth $1/\tau$ of a single receiver.

First, we provide an example of target detection with S-S-D-T compression. We consider a target scene with $L = 4$ targets distributed in the direction-range-velocity observation scene, whose reflectivities were all set to unity (see Fig. 2(a)). Two of the targets were placed on the grid while the others were off-grid. In every PRI, the number of frequency points transmitted by each transmitter was 4, i.e. a quarter of the whole bandwidth. The frequency points of the two transmitters were kept different from each other to ensure waveform orthogonality. To quantify the effect of dilution in the Doppler domain, we define the normalized aperture occupancy (NAO) as the AO di-

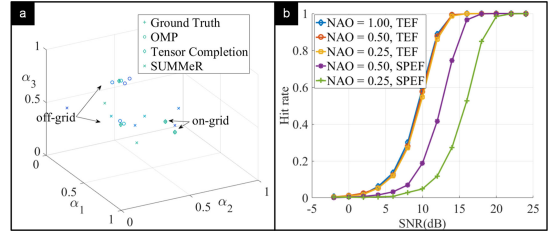


Fig. 2. (a) The recovered normalized delay-Doppler-DoA map. Detections via tensor-OMP, TC and SUMMeR are indicated by circles, diamonds, and oblique crosses respectively. The crosses indicate true location of the targets. (b) Hit rate comparison. The abbreviations TEF and SPEF stand for ‘total energy fixed’ and ‘single pulse energy fixed’, respectively.

vided by the whole transmit pulse product: $\text{NAO} = \frac{\sum_{m=0}^{M-1} P_m}{MP}$. In this experiment, each transmitter sent only 4 pulses implying $\text{NAO} = 0.25$. In comparison, the NAO of SUMMeR must be no less than 0.5. We apply the hit-or-miss criterion as the performance metric to compare tensor-OMP and TC. Here, a “hit” occurs when the estimated target is within one Nyquist bin defined as $2/(TR)$, $\tau/(TN)$, and $1/(P\tau)$ for the DoA, delay and Doppler, respectively - from the truth.

In Fig. 2(a), the on-grid targets are successfully detected by both OMP and TC. However, only TC showed successful detections of off-grid targets at the exact location while OMP found several solutions many bins away from the true target location. The Doppler-focusing-based SUMMeR recovery algorithm [22] fails to recover most of the targets.

Next, we placed $L = 2$ targets on the scene. Each pulse contained 4 frequency points. The hit rate was computed over 10,000 Monte-Carlo trials (see Fig. 2(b)). When the total transmit energy is the same, the reduction of AO does not significantly influence target detection. On the other hand, when the transmit energy in each pulse is fixed, performance deteriorates and the hit rate curve moves approximately 3 dB and 6 dB to the right for $\text{NAO} = 0.5$ and 0.25, respectively.

V. CONCLUSION

We proposed a new radar structure, TenDSuR, to recover a target scene consisting of range, Doppler and DoA at high resolution. Compared to a Nyquist MIMO radar, TenDSuR uses less spectral resources and operates at low complexity by exploiting tensor-based OMP and TC algorithms. In addition, the TC algorithm used in TenDSuR yields better accuracy for off-grid targets with respect to SUMMeR even without compression in the Doppler domain.

REFERENCES

- [1] H. Griffiths *et al.*, “Radar spectrum engineering and management: Technical and regulatory issues,” *Proc. IEEE*, vol. 103, no. 1, pp. 85–102, Jan. 2015.
- [2] K. V. Mishra and Y. C. Eldar, “Sub-Nyquist radar: Principles and prototypes,” 2018, arxiv:1803.01819.
- [3] D. Cohen and Y. C. Eldar, “Sub-Nyquist radar systems: Temporal, spectral and spatial compression,” *IEEE Signal Process. Mag.*, vol. 35, no. 6, pp. 35–58, Nov. 2018.
- [4] “Converged collaborative elements for RF task operations (CONCERTO),” DARPA Strategic Technol. Office, Arlington, VA, USA, Tech. Rep. DARPA-BAA-16-28, 2016.
- [5] K. V. Mishra, I. Kahane, A. Kaufmann, and Y. C. Eldar, “High spatial resolution radar using thinned arrays,” in *Proc. IEEE Radar Conf.*, 2017, pp. 1119–1124.

- [6] K. V. Mishra, A. Kruger, and W. F. Krajewski, "Compressed sensing applied to weather radar," in *Proc. IEEE Int. Geosci. Remote Sens. Symp.*, 2014, pp. 1832–1835.
- [7] D. Cohen, K. V. Mishra, and Y. C. Eldar, "Spectrum sharing radar: Coexistence via Xampling," *IEEE Trans. Aerosp. Electron. Syst.*, vol. 54, no. 3, pp. 1279–1296, Jun. 2018.
- [8] K. V. Mishra, A. Zhitnikov, and Y. C. Eldar, "Spectrum sharing solution for automotive radar," in *Proc. IEEE Veh. Technol. Conf.*, 2017, pp. 1–5.
- [9] K. V. Mishra *et al.*, "Cognitive sub-Nyquist hardware prototype of a collocated MIMO radar," in *Proc. Int. Workshop Compressed Sens. Theory Appl. Radar, Sonar, Remote Sens.*, 2016, pp. 56–60.
- [10] K. V. Mishra and Y. C. Eldar, "Performance of time delay estimation in a cognitive radar," in *Proc. IEEE Int. Conf. Acoust., Speech, Signal Process.*, 2017, pp. 3141–3145.
- [11] X. Wang, E. Aboutanios, M. Trinkle, and M. G. Amin, "Reconfigurable adaptive array beamforming by antenna selection," *IEEE Trans. Signal Process.*, vol. 62, no. 9, pp. 2385–2396, May 2014.
- [12] J. Liu, C. Han, X. Yao, and F. Lian, "Compressive sensing based track before detection algorithm for airborne radars," *Prog. Electromagn. Res.*, vol. 138, pp. 433–451, 2013.
- [13] V. Dang and O. Kilic, "Joint DoA-range-Doppler tracking of moving targets based on compressive sensing," in *Proc. IEEE Antennas Propag. Soc. Int. Symp.*, 2014, pp. 141–142.
- [14] R. A. Sevimli, M. Tofighi, and A. E. Cetin, "Range-Doppler radar target detection using denoising within the compressive sensing framework," in *Proc. Eur. Signal Process. Conf.*, 2014, pp. 1950–1954.
- [15] Y. C. Eldar, *Sampling Theory: Beyond Bandlimited Systems*. Cambridge, U.K.: Cambridge Univ. Press, 2015.
- [16] E. Baransky, G. Itzhak, I. Shmuel, N. Wagner, E. Shoshan, and Y. C. Eldar, "A sub-Nyquist radar prototype: Hardware and algorithms," *IEEE Trans. Aerosp. Electron. Syst.*, vol. 50, no. 2, pp. 809–822, Apr. 2014.
- [17] K. M. Cohen, C. Attias, B. Farbman, I. Tseleniker, and Y. C. Eldar, "Channel estimation in UWB channels using compressed sensing," in *Proc. IEEE Int. Conf. Acoust., Speech, Signal Process.*, 2014, pp. 1966–1970.
- [18] K. V. Mishra and Y. C. Eldar, "Sub-Nyquist channel estimation over IEEE 802.11ad link," in *Proc. IEEE Int. Conf. Sampling Theory Appl.*, 2017, pp. 355–359.
- [19] O. Bar-Ilan and Y. C. Eldar, "Sub-Nyquist radar via Doppler focusing," *IEEE Trans. Signal Process.*, vol. 62, no. 7, pp. 1796–1811, Apr. 2014.
- [20] D. Cohen and Y. C. Eldar, "Reduced time-on-target in pulse Doppler radar: Slow time domain compressed sensing," in *Proc. Radar Conf.*, 2016, pp. 1–4.
- [21] M. Rossi, A. M. Haimovich, and Y. C. Eldar, "Spatial compressive sensing for MIMO radar," *IEEE Trans. Signal Process.*, vol. 62, no. 2, pp. 419–430, Jan. 2014.
- [22] D. Cohen, D. Cohen, Y. C. Eldar, and A. M. Haimovich, "SUMMeR: Sub-Nyquist MIMO radar," *IEEE Trans. Signal Process.*, vol. 66, no. 16, pp. 4315–4330, Aug. 2018.
- [23] K. V. Mishra, Y. C. Eldar, E. Shoshan, M. Namer, and M. Meltsin, "A cognitive sub-Nyquist MIMO radar prototype," 2018, arxiv:1807.09126.
- [24] N. D. Sidiropoulos, L. Lathauwer, K. Fu, X. Huang, E. E. Papalexakis, and C. Faloutsos, "Tensor decomposition for signal processing and machine learning," *IEEE Trans. Signal Process.*, vol. 65, no. 13, pp. 3551–3582, Jul. 2017.
- [25] M. Haardt, F. Röemer, and G. D. Galdo, "Higher-order SVD-based subspace estimation to improve the parameter estimation accuracy in multidimensional harmonic retrieval problems," *IEEE Trans. Signal Process.*, vol. 56, no. 7, pp. 3198–3213, Jul. 2008.
- [26] F. Röemer, G. Del Galdo, and M. Haardt, "Tensor-based algorithms for learning multidimensional separable dictionaries," in *Proc. IEEE Int. Conf. Acoust., Speech, Signal Process.*, 2014, pp. 3963–3967.
- [27] M. Landmann, M. Kaske, and R. Thomä, "Impact of incomplete and inaccurate data models on high resolution parameter estimation in multidimensional channel sounding," *IEEE Trans. Antennas Propag.*, vol. 60, no. 2, pp. 557–573, Feb. 2012.
- [28] F. Wen, Z. Zhang, K. Wang, G. Sheng, and G. Zhang, "Angle estimation and mutual coupling self-calibration for ULA-based bistatic MIMO radar," *Signal Process.*, vol. 144, no. Supplement C, pp. 61–67, 2017.
- [29] Y. Yu, A. P. Petropulu, and H. V. Poor, "CSSF MIMO radar: Compressive-sensing and step-frequency based MIMO radar," *IEEE Trans. Aerosp. Electron. Syst.*, vol. 48, no. 2, pp. 1490–1504, Apr. 2012.
- [30] T. Huang, Y. Liu, H. Meng, and X. Wang, "Cognitive random stepped frequency radar with sparse recovery," *IEEE Trans. Aerosp. Electron. Syst.*, vol. 50, no. 2, pp. 858–870, Apr. 2014.
- [31] S. Gandy, B. Recht, and I. Yamada, "Tensor completion and low-n-rank tensor recovery via convex optimization," *Inverse Problems*, vol. 27, no. 2, 2011, Art. no. 025010.
- [32] J. Ying *et al.*, "Hankel matrix nuclear norm regularized tensor completion for n -dimensional exponential signals," *IEEE Trans. Signal Process.*, vol. 65, no. 14, pp. 3702–3717, Jul. 2017.
- [33] Y. C. Eldar and G. Kutyniok, *Compressed Sensing: Theory and Applications*. Cambridge, U.K.: Cambridge Univ. Press, 2012.